VHF/UHF Antenna Pattern Measurement with Unmanned Aerial Vehicles

Fabio Paonessa, Giuseppe Virone, Elisa Capello, Giuseppe Addamo, Oscar A. Peverini, Riccardo Tascone
Istituto di Elettronica ed Ingegneria dell'Informazione e delle Telecomunicazioni (IEIIT)
Consiglio Nazionale delle Ricerche (CNR)
C.so Duca degli Abruzzi 24, 10129, Torino, Italy
giuseppe.virone@ieiit.cnr.it

Pietro Bolli
Osservatorio Astrofisico di Arcetri (OAA)
Istituto Nazionale di Astrofisica (INAF)
Largo Enrico Fermi 5, 50125, Firenze, Italy

Giuseppe Pupillo, Jader Monari, Marco Schiaffino, Federico Perini, Simone Rusticelli
Istituto di Radio Astronomia (IRA)
Istituto Nazionale di Astrofisica (INAF)
Via Fiorentina 3513, 40059, Medicina (BO), Italy

Andrea M. Lingua, Marco Piras, Irene Aicardi, Paolo Maschio
Dipartimento di Ingegneria dell'Ambiente, del Territorio e delle Infrastrutture (DIATI)
Politecnico di Torino
C.so Duca degli Abruzzi 24, 10129, Torino, Italy

***Abstract*— The characterization of VHF and UHF antennas is very challenging owing to the very low-operative frequency. This paper presents a novel technique (originally developed for radio-astronomical applications) that can be suitable to measure ground-based aerospace antennas in real installation conditions, with an accurate and cost-effective method which does not require additional infrastructures. The system mainly consists of a micro Unmanned Aerial Vehicle (UAV), equipped with both a RF transmitter and an antenna, properly designed to operate as a far-field artificial test-source. Experimental results on a ground-based antenna at 50 MHz are provided. The extension of this technique to characterize service antennas (telemetry, remote control) onboard aerial vehicles is also reported. A measured pattern example of a 433 MHz telemetry monopole mounted on a commercial UAV is shown.**

Keywords—UAV; Antenna Measurements; VHF; UHF

I. INTRODUCTION

VHF and UHF antennas are widely used in communication and navigation systems for aeronautical applications, for both manned and unmanned aircraft. Some examples are the VHF Omnidirectional Range (VOR), operating from 108 MHz to 117.95 MHz, the Distance Measuring Equipment (DME), operating from 962 MHz to 1213 MHz, and the Instrument Landing System (ILS), operating from 75 MHz to 335.4 MHz. The satellite-based Automatic Identification System (AIS) also operates in the VHF range. Moreover, the same frequency range is used in meteor detection systems such as the Belgian Radio Meteor Stations (BRAMS) [1], operating around 50 MHz.

For all these systems, the characterization of the antenna radiation pattern is a very important task that should be performed in the real installation conditions. As well known, at these low operative frequencies, the pattern characterization cannot be accurately performed in anechoic chambers owing to their small size in terms of wavelength and the poor absorption characteristics of their walls. Moreover, outdoor test ranges (e.g. elevated or slanted) are quite large and expensive infrastructures which don't take into account the pattern distortions due to the real antenna installation conditions.

Recently, the authors developed an innovative technique for the characterization of the radiation pattern of VHF/UHF antennas [2]. Other interesting implementations of this concept can be found in [3]-[5]. The system described in section II is based on a flying artificial test source that was developed within the framework of the Square Kilometre Array (SKA) as part of the Italian contribution to this new international radio astronomical facility [6]-[8]. Such artificial source mainly consists of a battery-powered micro Unmanned Aerial Vehicle (UAV), equipped with a radio-frequency transmitter and a dipole antenna (Fig. 1).

In section III, the overall measurement strategy is applied to

Fig. 1. The flying test source consisting of the UAV equipped wih the RF transmitter and the dipole antenna operating at 50 MHz.

a dual-polarized Vivaldi antenna installed on the ground. The results at 50 MHz, which is a very challenging frequency for the traditional indoor and outdoor techniques are discussed from both the UAV positioning and the RF measurement point of views.

In section IV, the presented technique is extended to the characterization of antenna mounted on aerial vehicles. In particular, a ground-based antenna that has been already characterized according to the procedure in section III, is now used as a calibrated reference antenna. In this way, the radiation pattern of the onboard antenna-under-test can be easily extracted. An experimental example of a UAV-mounted monopole at 433 MHz is described.

II. System Description

A. Measurement System and Strategy

The UAV flies above the Antenna Under Test (AUT), which is placed on the ground, performing an autonomous GPS navigation (see Fig. 2). In particular, by defining consecutive waypoints, the UAV performs rectilinear flights above the AUT such as the two orthogonal trajectories shown in Fig. 3a (projection of such a cross-shaped path on the horizontal plane). The AUT is located in the center of the reference system, and the waypoints are the extremities of the cross.

During the flight, the drone position is measured with a dual-frequency Global Navigation Satellite System (GNSS) receiver using a Post Processed Kinematic (PPK) positioning, which provides centimeter accuracy. The continuous-wave radio frequency signal transmitted by the source (RF transmitter and dipole antenna) is received by the ground-based AUT allowing for its characterization in the real installation environment (on the soil, with mutual coupling due to adjacent structures etc.).

Assuming the AUT to be oriented such that the *E*-plane (which contains the electric field vector) coincides with the yz-plane and the *H*-plane coincides with the xz-plane, the two flight paths in Fig. 3a mainly correspond with the *E*- and *H*-plane cuts of the antenna radiation pattern. It should be pointed out that the system enables the antenna pattern characterization for several different scenarios ranging from single antenna to

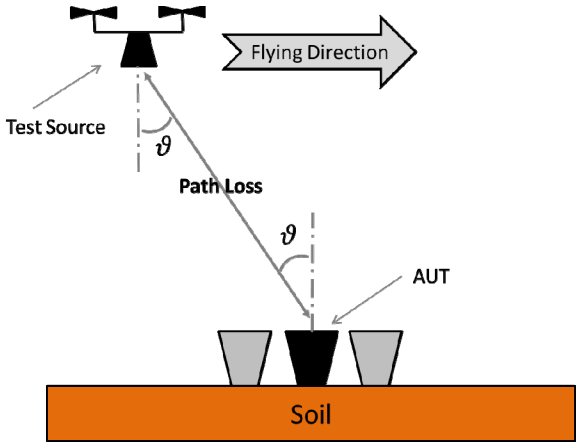

Fig. 2. Illustration of an embedded-element radiation pattern measurement.

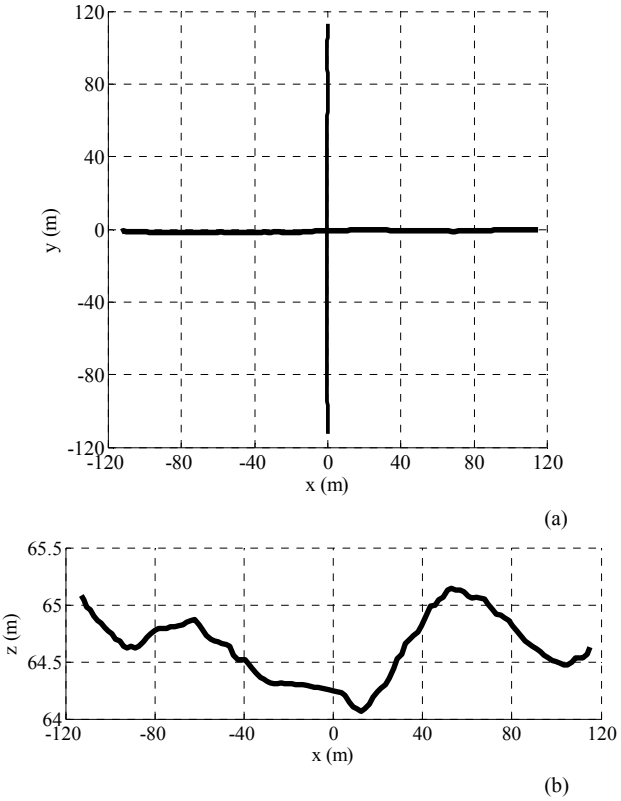

Fig. 3. (a) Flight paths projected on the horizontal plane, (b) flying height during the scan along the x-axis. The position data are measured by the differential GNSS receiver.

array of antennas. In this latter case, it is possible to measure both the embedded element pattern of each antenna and the beam-formed array pattern.

Usually, the programmed flying height is constant and it depends on the minimum far-field distance required, which is imposed by the operative frequency and the antenna size. It should be noted that the real flight path is different (few meters) from the programmed one, owing to the uncertainty of the internal onboard GPS and its navigation system. Therefore, as mentioned above, the real path is not perfectly coincident with the *E*- or *H*-plane of the radiation pattern. However, such a discrepancy is kept into account in the procedure for pattern extraction (section II.B).

Co- or cross-polarization measurements are performed by programming the proper UAV bearing angle, as a constant during the flight. When the UAV is at zenith, the bearing corresponds to the angle between the co-polarization directions of the test source and the AUT, measured on the horizontal plane. Therefore, the bearing is programmed either to 0 deg (co-polar) or 90 deg (cross-polar). It should be noted that during the flight, the orientation of the UAV has some variations, but these are measured by the on-board Inertial Measurement Unit (IMU) and kept into account in the procedure for pattern extraction.

B. Radiation Pattern Extraction Procedure

In the far-field condition, the power received by the AUT is described by the Friis transmission equation. Expressing all the quantities in decibel for convenience:

$$P_R(\underline{r}) = g_{AUT}(\mathbf{r}) + g_S(\mathbf{r},\alpha,\beta,\gamma) - P_L + P_S + G_R + \chi(\mathbf{r},\alpha,\beta,\gamma) \quad (1)$$

where P_R is the received power (measured quantity), which depends on the distance vector $\underline{r} = R\mathbf{r}$ from the AUT to the UAV ($\underline{r}$ is measured by the differential GNSS); g_{AUT} is the gain of the AUT (unknown quantity) along the specific observation direction $\mathbf{r}$ (unit vector); g_S is the gain of the test-source, which depends both on the direction $\mathbf{r}$ and on the UAV orientation described by the Euler angles α, β, and γ, named yaw (or bearing), pitch and roll, respectively (these angles are measured by the IMU). Then $P_L = 20\mathrm{Log}_{10}(4\pi R/\lambda)$ is the path loss which depends on the wavelength λ and the distance R; P_S is the power radiated by the test source (i.e. the dipole mounted on the UAV); G_R is the sum of constant gains and attenuations along the chain up to the receiver input (cables, LNAs etc.). Finally, χ is the polarization mismatch factor, which depends both on the UAV position and its orientation:

$$\chi(\mathbf{r},\alpha,\beta,\gamma) = |\mathbf{p}_{AUT}(\mathbf{r}) \cdot \mathbf{p}_S(\mathbf{r},\alpha,\beta,\gamma)|^2 \quad (2)$$

where $\mathbf{p}_{AUT}$ and $\mathbf{p}_S$ are the polarization unit vectors of the AUT and the test source, respectively.

The AUT radiation pattern is extracted from (1) by means of the procedure described in [9]. In order to increase both the accuracy and the repeatability of measurements performed with moderate wind, the real (measured) values of both the orientation angles and the UAV position are used.

III. Experimental Results on a Ground-Based Antenna

This section presents an experimental verification of the Vivaldi antenna for the Sardinia Array Demonstrator (SAD) at 50 MHz. The measured data at higher frequencies are already reported in [10]. SAD is a national project of the Italian National Institute for Astrophysics (INAF), developed in parallel to the commitment inside SKA to improve the know-how in the area of aperture arrays for low-frequency radio astronomical research and test different architectural solutions [7] [11]. SAD consists of 128 dual-polarized Vivaldi antennas that will be deployed with a versatile approach able to recombine different array configurations. A Vivaldi antenna with gridded wings was designed for SAD (Fig. 4), this light version provides robustness against strong wind blasts, maintaining at the same time satisfactory electromagnetic performance.

Fig. 4. The dual-polarized Vivaldi antenna on the measurement field.

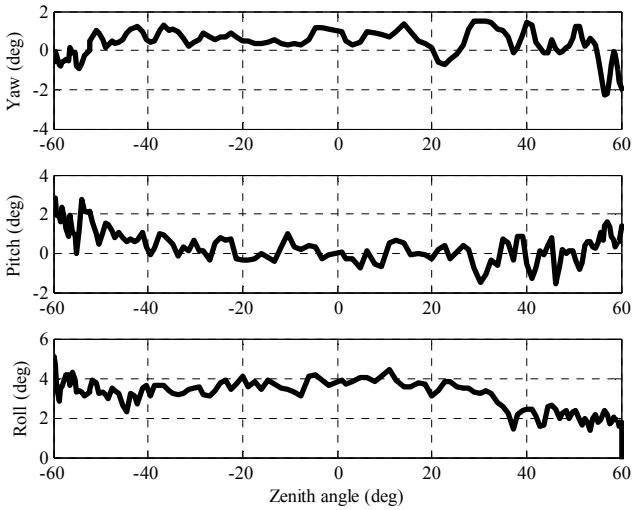

Fig. 5. Orientation of the UAV during the scan along the x-axis of Fig. 3a.

The antenna prototype characterization was performed by using the innovative UAV-based system. The corresponding results are reported hereinafter to give insight in the measurement procedure and the achievable accuracy. It should be noted that the same procedure can be directly applied to the aerospace antenna systems described in the introduction.

Figs. 3a and 3b show the position data of the UAV measured by the differential GNSS system. During the flight along the x-axis of Fig. 3a, the flying height was approximately 65 m (plot in Fig. 3b). The resulting angular scan was about ±60 deg with respect to the vertical direction. The two polarizations of the AUT were aligned with the x- and y-axes. The orientation angles of the test-source are instead shown in Fig. 5 (for the flight along the x-axis), note that the roll is approximately 4 deg, whereas pitch and yaw are close to their ideal values.

Fig. 6a shows the received power pattern for both the polarizations of the antenna. From these quantities, the radiation patterns are extracted. Fig. 6b shows the contributions of (1) (P_S and G_R are omitted). Note that the path loss reaches the minimum at zenith and increases for other angles, owing to the constant-height flight. The gain of the source antenna is almost constant, because it nearly corresponds to the gain of the source dipole, which is almost uniform at 50 MHz in the *H*-plane. Moreover, the polarization mismatch is 0 dB for the co-polar measurement (solid line) and much lower for the cross-polar one (dashed curve).

The extracted AUT radiation pattern is finally shown in Fig. 6c (solid and dashed lines). It is associated to the scan along the x-axis of Fig. 3a. As a consequence, the measurement provides an *E*-plane cut for the AUT x-polarization, and an *H*-plane cut for the y-polarization. Since the source dipole is oriented along the y-axis (yaw 0 deg), the co-polar pattern pertains to the y-polarization. On the contrary, the cross-polar pattern pertains to the x-polarization.

A full-wave electromagnetic simulation of the AUT was performed and compared to the measured pattern, since no other reference measured data were available (see introduction). The two curves are in good agreement, and the discrepancy is within 0.3 dB. This small difference can be explained by many factors, e.g. a) uncertainties of the EM modeling of the AUT and its interaction with the soil, b) mechanical uncertainties of the AUT position and orientation on the ground, c) uncertainties of the measured UAV orientation during the flight.

The measured cross-polar level is instead lower than -20 dB. The cross-polar simulation is not shown being very low for this antenna at 50 MHz. In this case, uncertainties of the test source position and orientation, bearing in particular, are predominant [12].

IV. Experimental Results on a UAV-Mounted Antenna

Besides the intrinsic interest about measuring VHF/UHF antennas on the ground for the specific applications mentioned in the introduction, the present UAV-based measurement system can be used to characterize (calibrate) a set of ground-based reference antennas that can be useful in many other scenarios. For example, the log-periodic antenna shown in Fig. 7 has been extensively characterized in previous campaigns [2] [12]. In this work, such an antenna is used as a known reference for the characterization of the short telemetry monopole at 433 MHz onboard the commercial UAV shown in Fig. 8 (3DR X8+). The flying strategy is similar to the one described in section II. The extraction procedure can be easily obtained from (1) considering the parameter g_S as the unknown.

Two measured results obtained with different flights in the same operative conditions are reported in Fig. 9. The repeatability is within 1 dB. A simulated curve is not available since the geometry of the telemetry monopole (quarter wave helix embedded in a plastic cover) is not fully known. However, the measured pattern in Fig. 9 is basically consistent with the expected quarter-wave monopole structure oriented toward the ground. Even if the monopole was vertically oriented, the position of the minimum is 20 deg far from the nadir direction. This offset is certainty related to the presence of all the metallic parts of the micro UAV (arm, circuit boards and wires) which operate as an asymmetrical ground plane for the monopole. This measured result also highlights that the coverage of a monopole antenna mounted on a micro-UAV is very far from optimum, i.e. it is not uniform across the observation angle and the power level at -20 deg is very low.

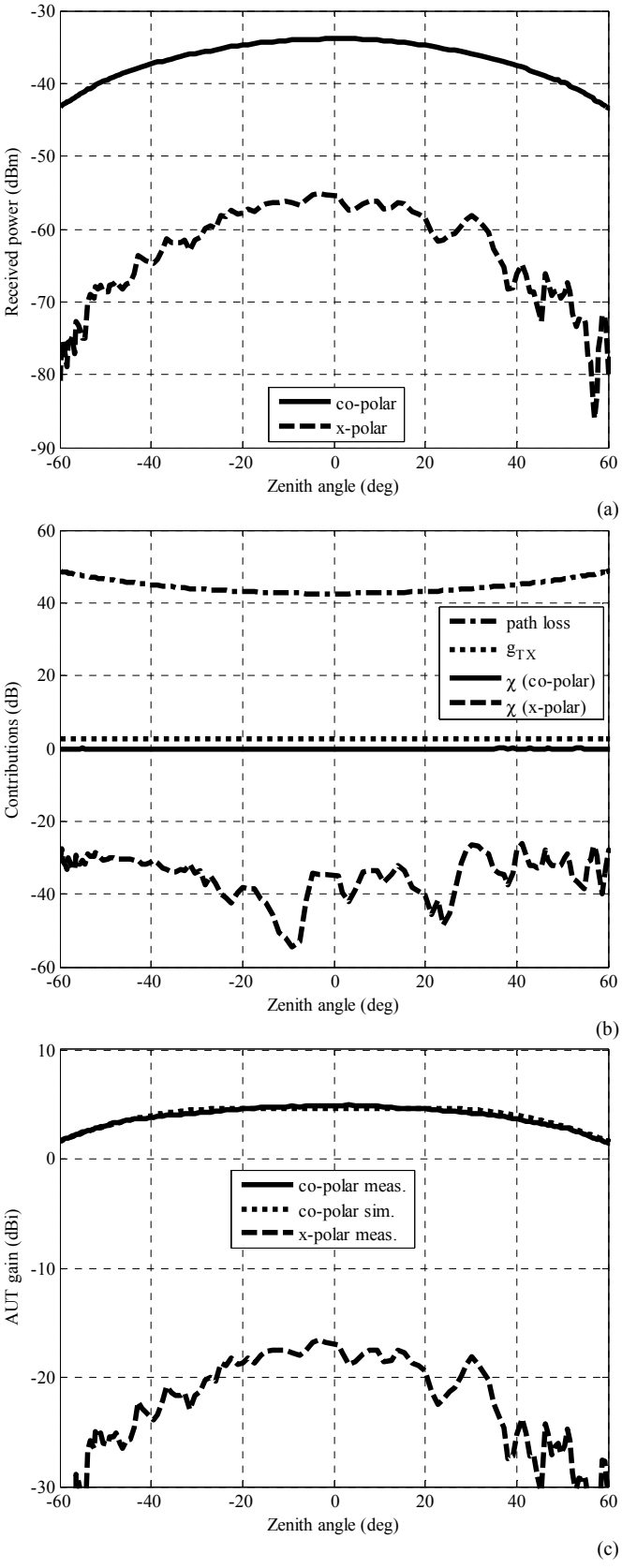

Fig. 6. (a) Received power pattern, (b) contributions of the Friis formula, (c) extracted AUT radiation pattern.

Fig. 7. The log-periodic antenna used as a known reference for the characterization of the telemetry monopole onboard the UAV.

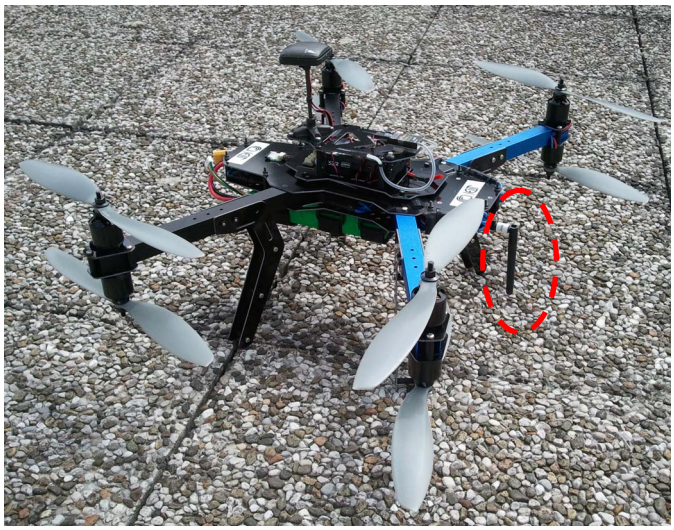

Fig. 8. Antenna Under Test (red dashed contour) mounted on a commercial micro UAV (3DR X8+).

V. Conclusion

A UAV-based innovative system for the characterization of VHF and UHF antennas has been developed within the framework of SKA to characterize elements and arrays for low frequency radio astronomy. However, we have shown that this system is suitable also for aerospace and other kind of applications involving antenna measurements in these frequency bands. Excellent results have been obtained at 50 MHz, a frequency that poses several problems to the traditional measurement systems due to the strong interaction with the soil and the adjacent structures.

The strategy has been extended to radiation pattern measurement of UAV-mounted service antennas. The obtained results clearly show the weakness of a commonly adopted telemetry antenna configuration.

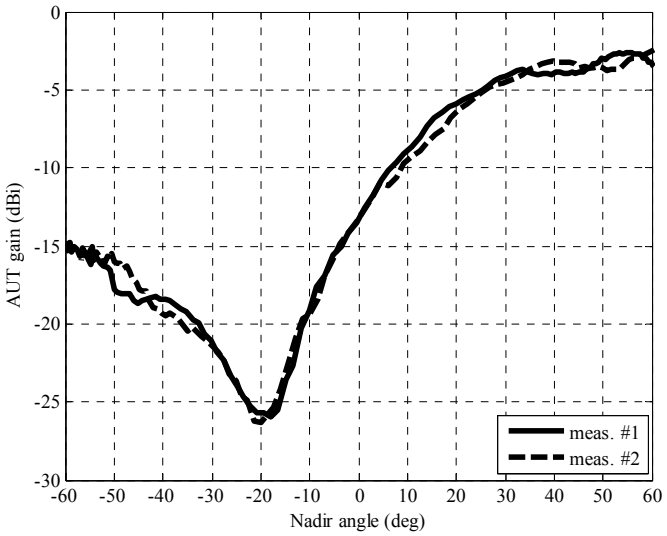

Fig. 9. Measured telemetry monopole pattern at 433 MHz.

References

[1] S. Ranvier, et al., "Instrumentation of the Belgian radio meteor stations (BRAMS)," International Conference on Electromagnetics in Advanced Applications (ICEAA), Sept. 7-11 2015, Turin, Italy.

[2] G. Virone, et al., "Antenna pattern verification system based on a micro unmanned aerial vehicle (UAV)," IEEE Antennas and Wireless Propagation Letters, vol.13, pp. 169-172, Jan. 2014.

[3] F. Üstüner, et al. "Antenna Radiation Pattern Measurement Using an Unmanned Aerial Vehicle (UAV)", General Assembly and Scientific Symposium (URSI GASS), 2014 XXXIth URSI, 16-23, Beijing. China, Aug. 2014

[4] A. Martínez Picar, et al. "Antenna Pattern Calibration of Radio Telescopes using an UAV-based device", International Conference on Electromagnetics in Advanced Applications (ICEAA), Sept. 7-11 2015, Turin, Italy.

[5] C. Chang, et al. "Beam Calibration of Radio Telescopes with Drones", Publications of the Astronomical Society of the Pacific, 127:000–000, Nov. 2015.

[6] G. Pupillo, et al., "Medicina array demonstrator: calibration and radiation pattern characterization using a UAV-mounted radio-frequency source," Experimental Astronomy, vol. 39, pp. 405-421, Apr. 2015.

[7] P. Bolli, et al. "From MAD to SAD: The Italian experience for the low-frequency aperture array of SKA1-LOW", Radio Sci., 51, 160–175, doi:10.1002/2015RS005922, Mar 2016.

[8] F. Paonessa, et al., "UAV-based pattern measurement of the SKALA," IEEE Antennas and Propagation Society International Symposium (APSURSI), July 19-25 2015, Vancouver, Canada.

[9] G. Virone, et al., "Antenna pattern measurements with a flying far-field source (hexacopter)," IEEE International Conference on Antenna Measurements and Applications, Nov. 16-19 2014, Antibes Juan-les-Pins, France.

[10] P. Bolli, et al., "Sardinia Aperture Array Demonstrator: Electromagnetic Analysis and Measurements," 36th ESA Antenna Workshop on Antennas and RF Systems for Space Science, Oct. 6-9 2015, Noordwijk, the Netherlands.

[11] P. Bolli, et al., "Sardinia array demonstrator: instrument overview and status," International Conference on Electromagnetics in Advanced Applications (ICEAA), Sept. 7-11 2015, Turin, Italy.

[12] F. Paonessa, et al., "Antenna Pattern Measurement with UAVs: Cross Polarization Performance," 36th ESA Antenna Workshop on Antennas and RF Systems for Space Science, Oct. 6-9 2015, Noordwijk, the Netherlands.